Published online: March 5, 2018

Article

TRANSPARENT PROCESS

EMBO reports

Zc3h10 is a novel mitochondrial regulator

Matteo Audano[1], Silvia Pedretti[1], Gaia Cermenati[1], Elisabetta Brioschi[1], Giuseppe Riccardo Diaferia[2], Serena Ghisletti[3], Alessandro Cuomo[2], Tiziana Bonaldi[2], Franco Salerno[4], Marina Mora[4], Liliana Grigore[5,6], Katia Garlaschelli[6], Andrea Baragetti[1,6], Fabrizia Bonacina[1], Alberico Luigi Catapano[1,5], Giuseppe Danilo Norata[1,6,7], Maurizio Crestani[1], Donatella Caruso[1], Enrique Saez[8], Emma De Fabiani[1,*] & Nico Mitro[1,**]

Abstract

Mitochondria are the energy-generating hubs of the cell. In spite of considerable advances, our understanding of the factors that regulate the molecular circuits that govern mitochondrial function remains incomplete. Using a genome-wide functional screen, we identify the poorly characterized protein Zinc finger CCCH-type containing 10 (Zc3h10) as regulator of mitochondrial physiology. We show that Zc3h10 is upregulated during physiological mitochondriogenesis as it occurs during the differentiation of myoblasts into myotubes. Zc3h10 overexpression boosts mitochondrial function and promotes myoblast differentiation, while the depletion of Zc3h10 results in impaired myoblast differentiation, mitochondrial dysfunction, reduced expression of electron transport chain (ETC) subunits, and blunted TCA cycle flux. Notably, we have identified a loss-of-function mutation of Zc3h10 in humans (Tyr105 to Cys105) that is associated with increased body mass index, fat mass, fasting glucose, and triglycerides. Isolated peripheral blood mononuclear cells from individuals homozygotic for Cys105 display reduced oxygen consumption rate, diminished expression of some ETC subunits, and decreased levels of some TCA cycle metabolites, which all together derive in mitochondrial dysfunction. Taken together, our study identifies Zc3h10 as a novel mitochondrial regulator.

Keywords functional screens; metabolism; mitochondria; Zc3h10
Subject Categories Metabolism; Molecular Biology of Disease
DOI 10.15252/embr.201745531 | Received 22 November 2017 | Revised 2 February 2018 | Accepted 7 February 2018 | Published online 5 March 2018
EMBO Reports (2018) 19: e45531

Introduction

Mitochondria generate ATP to support a plethora of cellular functions. As such, mitochondria are essential for the normal functioning of cells [1]. Hence, it is not surprising that mitochondrial dysfunction has been associated with multiple human pathologies [2]. Defects in mitochondrial function can be the result of an inadequate number of structurally sound mitochondria, an inability to deliver substrates to the organelle, or abnormalities in the electron transport chain (ETC) and/or oxidative phosphorylation (Oxphos) [3–6]. There is great interest in identifying approaches to restore mitochondrial function in disease, as it is thought that this may offer therapeutic benefit [7]. Progress toward this goal, however, has been hampered by our limited knowledge of the molecular mechanisms that control mitochondrial number and function.

Mitochondria possess their own genome, which encodes 2 rRNAs, 22 tRNAs, and 13 proteins that are part of the electron transport chain. Mitochondrial DNA (mtDNA) replication and transcription are under the primary control of mitochondria transcription factor A (Tfam), a nuclear-encoded transcription factor critical for mitochondrial biogenesis and function [8]. Tfam is only one of ~1,200 mitochondrial proteins encoded in the nucleus [9], an observation that highlights the tight relationship between the nucleus and mitochondria. The interdependence of these organelles is also evidenced by the fact that metabolites generated in mitochondria are required for many nuclear functions, such as DNA replication, RNA transcription, splicing, and cytoplasmic/nuclear transport [10–13]. Tfam expression is regulated by a battery of transcription factors and cofactors (e.g., Pgc-1α, Pgc-1β, Pparγ, Pparα, Errα, YY1, and others), many of which have been shown to play important roles in mitochondrial activity [7,14,15]. It is likely that other unidentified regulators of Tfam, if they exist, will also have a significant impact on mitochondrial physiology.

1 DiSFeB, Dipartimento di Scienze Farmacologiche e Biomolecolari, Università degli Studi di Milano, Milan, Italy
2 Department of Experimental Oncology, European Institute of Oncology (IEO), Milan, Italy
3 Humanitas Clinical and Research Center, Rozzano-Milan, Italy
4 Neuromuscular Diseases and Neuroimmunology Unit, Foundation IRCCS C. Besta Neurological Institute, Milan, Italy
5 IRCSS Multimedica, Milan, Italy
6 SISA Centre, Bassini Hospital, Cinisello Balsamo, Italy
7 School of Biomedical Sciences, Curtin Health Innovation Research Institute, Faculty of Health Science, Curtin University, Perth, WA, Australia
8 Department of Molecular Medicine, The Scripps Research Institute, La Jolla, CA, USA
*Corresponding author. Tel: +39 02 50318323; E-mail: emma.defabiani@unimi.it
**Corresponding author. Tel: +39 02 50318253; E-mail: nico.mitro@unimi.it

In this work, we have used the Tfam promoter as a platform to identify new regulators of mitochondria number and function. Using a genome-wide overexpression screen followed by assays of mitochondrial number and activity, we have identified Zinc finger CCCH-type containing 10 (Zc3h10) as a new regulator of mitochondrial physiology.

Here, we have applied an integrated approach (genomics, transcriptomics, proteomics, metabolomics, cell-based assays, human genetics) to show that Zc3h10 regulates mitochondrial physiology. Further, stressing the physiologic relevance of our findings, we have identified a Zc3h10 loss-of-function mutation in humans that results in mitochondrial dysfunction and is associated with adverse metabolic traits (e.g., increased body mass index, fasting glucose, and triglyceride levels).

Results

Functional screen to isolate regulators of mitochondrial function

To identify new factors that regulate mitochondrial activity, we performed a genome-wide functional screen in which cDNAs for 16,000 genes (MGCv2) were individually transfected into HEK293 cells together with a luciferase reporter that registers the activity of the mitochondrial transcription factor a (Tfam) promoter (Fig 1A). Tfam selectively regulates mitochondrial (mt) transcription and mtDNA replication and is essential for mitochondrial biogenesis [8]. This reporter construct responds appropriately to known positive and negative regulators of mitochondrial function (Fig 1A top left inset) such as peroxisome proliferator-activated receptor γ coactivator-1α (Pgc-1α) and Myb binding protein 1a (Mybbp1a), respectively [16,17]. From this primary screen, 440 cDNAs (348 positive and 92 negative hits) were selected for validation based on their ability to modulate Tfam promoter activity to a similar or greater extent than the positive (Pgc-1α) and negative (Mybbp1a) controls, and on their expression in metabolic tissues (skeletal muscle, liver, pancreas, and adipose tissues) (Fig 1B). Primary hits were evaluated in a secondary screen in which HEK293 cells individually transfected with putative mitochondrial regulators were stained with Mitotracker Green and Mitotracker Red CM-H_2XRos as readouts of mitochondrial density and function respectively and analyzed by FACS (secondary screen, Fig 1A). This analysis yielded 126 positive and 32 negative hits that modulated mitochondrial density and function to a similar or greater extent than the positive (Pgc-1α) and negative (Mybbp1a) controls (Fig 1C). Tissue set enrichment analysis revealed that confirmed positive hits from this latter screen were primarily expressed in muscle (Fig EV1A). We selected 21 positive hits based on their expression in skeletal muscle and C2C12 myotubes (Fig EV1B), their lack of prior association with mitochondrial biology, and the diversity of protein classes they represented (Fig EV1C), for further validation. The ability of these potential positive regulators of mitochondrial function to increase mtDNA content and basal respiration was tested in C2C12 myoblasts (tertiary screen, Fig 1A). In these assays, Zc3h10 emerged as the factor with the greatest ability to enhance mitochondrial functional parameters (Figs 1D and EV1D). Zc3h10, a poorly characterized protein, is expressed in male and female human quadriceps, and ubiquitously in mouse and human tissues (Fig EV1E and F).

Overexpression of Zc3h10 in C2C12 myoblasts (Fig EV1G) increased Tfam promoter activity (Fig 1E), Tfam mRNA and protein expression (Fig 1F and G), and protein levels of several Oxphos subunits (Fig 1G). Notably, overexpression of Zc3h10 boosted cellular respiration (Fig 1H) and ATP production (Fig 1I) to a similar degree as overexpression of Pgc-1α. Despite inducing a significant increase in oxygen consumption, overexpression of Zc3h10 did not augment reactive oxygen species levels or apoptosis (Fig EV1H).

Zc3h10 is a new regulator of mitochondrial function

To examine the role of Zc3h10 in a physiologic setting characterized by increased mitochondrial biogenesis, we studied its expression during the differentiation of C2C12 myoblasts into myotubes. Expression of Zc3h10 mRNA (Fig 2A) paralleled the increases in

Figure 1. High-throughput screen to identify a new regulator of mitochondrial function.

A A genome-wide primary screen testing the ability of individual cDNAs to control *Tfam* promoter activity was performed in HEK293 cells. Top left inset shows performance of controls. Hits were filtered in a secondary screen measuring mitochondrial density and function in HEK293 cells. Validated positive hits were further evaluated for their ability to increase mitochondrial respiration and mtDNA levels in C2C12 myoblasts.

B Scatter plot of primary screen data in HEK293 cells. Hits were selected based on their inhibitory or stimulatory effect on *Tfam* promoter activity relative to known negative (Mybbp1a) and positive (Pgc-1α) *Tfam* regulators.

C Scatter plot of secondary screen results in HEK293 cells. 126 positive and 32 negative hits controlled mitochondrial function to a similar or greater extent than the Pgc-1α and Mybbp1a controls.

D Scatter plot of tertiary screen data in C2C12 myoblasts. Confirmed positive hits (21) from the secondary screen were transiently overexpressed in C2C12 myoblasts, and mtDNA levels and basal cell respiration were measured. Zc3h10 surfaced as a prime candidate for follow up studies.

E C2C12 myoblasts were co-transfected with indicated plasmids, and luciferase activity was evaluated 48 h later. $n = 3$. Statistical analysis was performed by one-way ANOVA with Dunnett's post-test vs. Tfam-Luc control. $^{***}P < 0.001$.

F *Tfam* mRNA levels 24 h after Pgc-1α and Zc3h10 overexpression in C2C12 myoblasts. $n = 4$. Statistical analysis was performed by one-way ANOVA with Dunnett's post-test vs. control. $^{**}P < 0.01$.

G Western blot analysis of indicated Oxphos subunits and Tfam 24 h after Pgc-1α and Zc3h10 overexpression in C2C12 myoblasts.

H Basal, uncoupled (Oligo), and maximal uncoupled (CCCP) respiration in control, Pgc-1α, and Zc3h10 overexpressing C2C12 myoblasts. $n = 3$. Statistical analysis was performed by one-way ANOVA with Dunnett's post-test. $^{**}P < 0.01$, $^{***}P < 0.001$ vs. basal control; $^{\$\$}P < 0.01$ vs. oligomycin control; $^{\#}P < 0.05$ vs. CCCP control.

I Cytosolic, mitochondrial, and total ATP levels 24 h after Pgc-1α and Zc3h10 transfection in C2C12 myoblasts. $n = 5$. Statistical analysis was performed by one-way ANOVA with Dunnett's post-test. $^{***}P < 0.001$ vs. mitochondrial control; $^{\$}P < 0.05$, $^{\$\$}P < 0.01$ vs. total control.

Data information: *n* indicates the number of biological replicates. Data are expressed as mean ± SD, and *P*-values were calculated from the indicated *n* independent experiments according to [44].

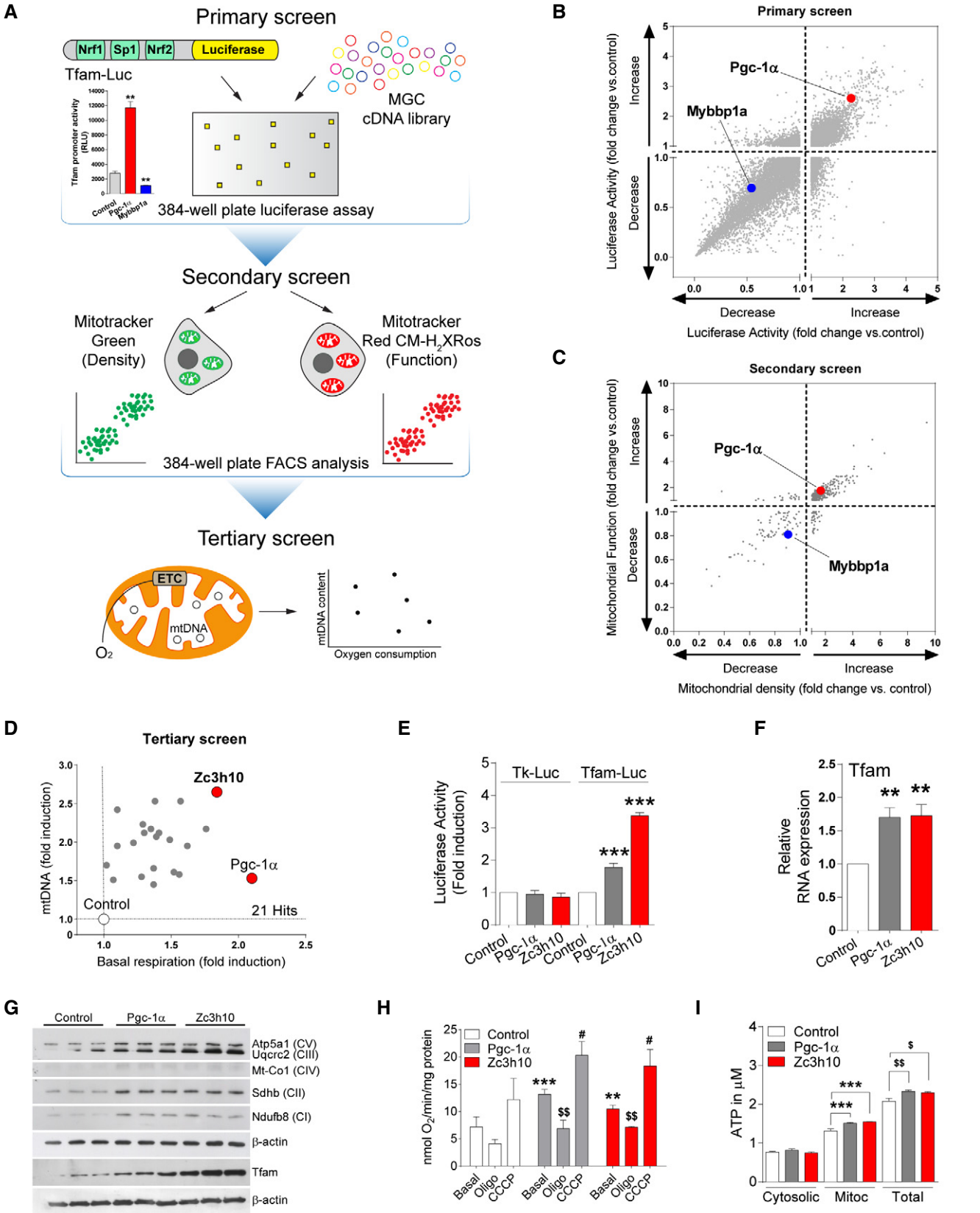
A
Primary screen
Nrf1
Sp1
Nrf2
Luciferase
Tfam-Luc
MGC
cDNA library
384-well plate luciferase assay
Secondary screen
Mitotracker
Green
(Density)
Mitotracker
Red CM-H2XRos
(Function)
384-well plate FACS analysis
Tertiary screen
ETC
mtDNA
O2
mtDNA content
Oxygen consumption
B
Primary screen
Pgc-1α
Mybbp1a
Increase
Decrease
Luciferase Activity (fold change vs.control)
C
Secondary screen
Pgc-1α
Mybbp1a
Mitochondrial Function (fold change vs.control)
Mitochondrial density (fold change vs. control)
D
Tertiary screen
Zc3h10
Pgc-1α
Control
21 Hits
mtDNA (fold induction)
Basal respiration (fold induction)
E
Tk-Luc
Tfam-Luc
Luciferase Activity (Fold induction)
F
Tfam
Relative RNA expression
G
Control
Pgc-1α
Zc3h10
Atp5a1 (CV)
Uqcrc2 (CIII)
Mt-Co1 (CIV)
Sdhb (CII)
Ndufb8 (CI)
β-actin
Tfam
β-actin
H
nmol O2/min/mg protein
Basal
Oligo
CCCP
I
ATP in μM
Cytosolic
Mitoc
Total

Figure 1.

Published online: March 5, 2018
EMBO reports

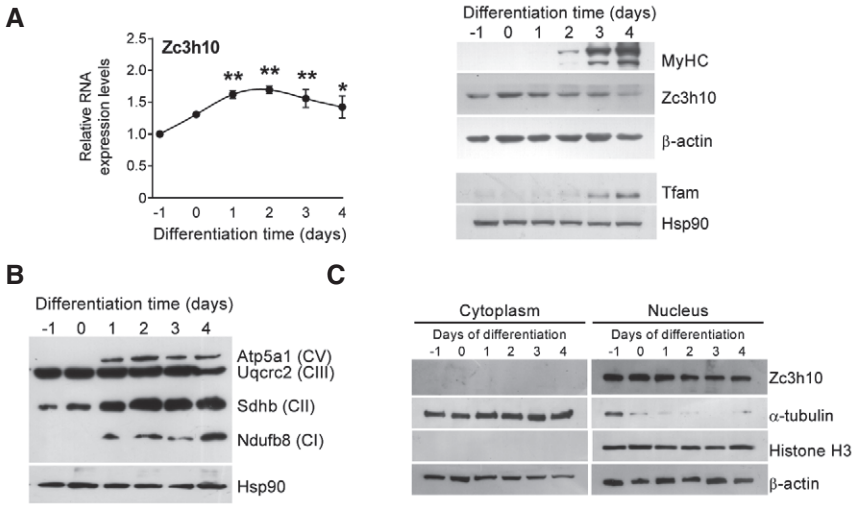

Figure 2. Zc3h10 is a nuclear protein upregulated during C2C12 differentiation.

A *Zc3h10* mRNA levels, Zc3h10, MyHC, and Tfam protein levels during C2C12 differentiation. Hsp90 and β-actin were used as loading controls. mRNA/n = 3. Statistical analysis was performed by one-way ANOVA with Dunnett's post-test. *$P < 0.05$, **$P < 0.01$ vs. day −1.

B Western blot analysis of indicated Oxphos subunits and Tfam during C2C12 differentiation.

C Western blot analysis to detect Zc3h10, α-tubulin, histone H3, and β-actin at different time points of C2C12 differentiation in both cytoplasm and nucleus. α-tubulin, histone H3, and β-actin were used as cytoplasmic, nuclear, and loading controls, respectively.

Data information: n indicates the number of biological replicates. Data are expressed as mean ± SD, and P-values were calculated from the indicated n independent experiments according to [44].

mtDNA content and *Tfam* (Figs EV2A and 2A) and Oxphos subunit expression (Fig 2B) known to accompany this process [18–20]. In differentiating C2C12 myoblasts, Zc3h10 is primarily, if not exclusively, localized in the nucleus (Fig 2C), with mRNA and protein levels increasing early during differentiation about twofold and declining in mature myotubes (Fig 2A and C). However, the observed discrepancy between Zc3h10 mRNA and protein levels during C2C12 differentiation may be likely due to possible post-transcriptional and/or post-translational mechanisms as already described for other proteins [21]. Interestingly, the increase in Zc3h10 expression mirrored the induction of the early myogenic factors *MyoD* and preceded the expression of MyHC (labeled as *MyHC7*), *Tnni1*, and *Mef2c* (Fig EV2A), markers of fully differentiated myotubes.

To assess the contribution of Zc3h10 to the increase in mitochondrial biogenesis and activity that characterizes the myogenic program, we used adenoviral infection to overexpress Zc3h10 in proliferating myoblasts (Fig EV2B). Mild overexpression of Zc3h10 in myoblasts (Fig EV2C and D) to mimic that found during C2C12 differentiation (Fig 2A, day 0) boosted mitochondrial activity and mtDNA content at different time points after the induction of differentiation (Fig 3A). Moreover, basal, uncoupled, and maximal uncoupled respiration and complex I, II, and IV activities were all increased 48 h after the induction of differentiation (Fig 3B). These functional increases were accompanied by higher levels of expression of mitochondrial and myogenic genes (Fig EV2E). Furthermore, overexpression of Zc3h10 in myoblasts had no effect on proliferation but strongly stimulated myotube formation, as reflected in a robust induction of the myofiber fusion index 72 h after induction of differentiation (day 3, Fig EV2F).

Next, we used a similar approach to knockdown Zc3h10 in proliferating myoblasts (Fig EV3A). Adenovirus-mediated ShRNA silencing of Zc3h10 in proliferating myoblasts led to a 50% reduction in Zc3h10 mRNA and protein 48 h after infection (Fig EV3B and C). This resulted in reduced expression of some Oxphos subunits (Fig 4A) and decreased basal, uncoupled, and maximal uncoupled respiration (Fig 4B). Similar results were observed in isolated mitochondria (Figs 4C and D, and EV3D). Interestingly, mtDNA content was not affected (Fig EV3E). Using the same protocol, we next analyzed the effect of Zc3h10 knockdown at 24, 48, and 72 h after the induction of myogenic differentiation. Zc3h10 knockdown (~50%; Fig EV3F and G) decreased the protein levels of Tfam and some Oxphos subunits (Fig 4E and F), and significantly reduced mitochondrial activity, as reflected in decreased basal respiration (Fig 4G). Total mtDNA content was unchanged (Fig EV3H). Basal, uncoupled, and maximal uncoupled respiration, complex I, II, and IV activities (Fig 4H and I), and ATP levels (Fig 4J) were all reduced in Zc3h10-silenced myotubes 48 h after induction of differentiation. RNA microarray profiling of these cells and Gene Set Enrichment Analysis (GSEA) confirmed that Zc3h10 is positively associated with mitochondria (Fig EV3I). Furthermore, knockdown of Zc3h10 in myoblasts significantly delayed myotube formation 72 h after induction of differentiation (day 3), as evidenced by a strong reduction in the myofiber fusion index in the absence of a proliferation rate difference (Fig 4K).

Together, these data demonstrate that Zc3h10 is a new regulator of mitochondria, one that is particularly important for proper mitochondriogenesis and increased mitochondrial activity during the early phase of myoblast to myotube differentiation.

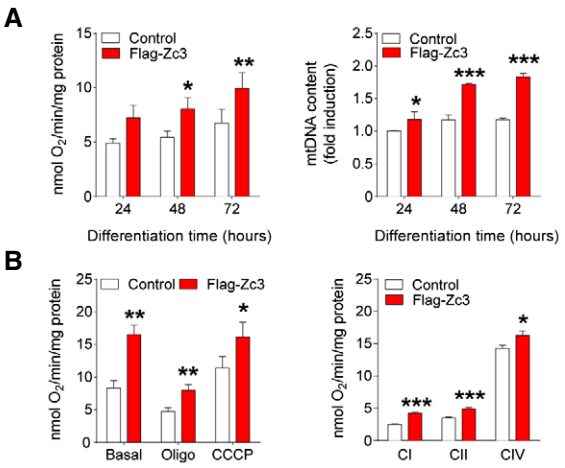

Figure 3. Zc3h10 overexpression boosts mitochondrial function and density in myotubes.

A Basal oxygen consumption and mtDNA content in control and Flag-Zc3h10-infected C2C12 myotubes 24, 48, and 72 h from differentiation induction. $n = 3$. Statistical analysis was performed by two-way ANOVA with Sidak post-test. $^{*}P < 0.05$, $^{**}P < 0.01$, $^{***}P < 0.001$ vs. control.

B Basal, uncoupled, and maximal uncoupled respiration and complex I, II, and IV activity evaluation 48 h from differentiation induction in control and Flag-Zc3h10 myotubes. $n = 3$. Statistical analysis was performed by Student's t-test. $^{*}P < 0.05$, $^{**}P < 0.01$, $^{***}P < 0.001$ vs. control.

Data information: n indicates the number of biological replicates. Data are expressed as mean ± SD, and P-values were calculated from the indicated n independent experiments according to [44].

Depletion of Zc3h10 results in ETC defects and decreased TCA cycle flux

To establish the relevance of Zc3h10 in mitochondrial biology, we next applied global proteomic and metabolomic approaches. Proteomic analysis using quantitative mass spectrometry (i.e., stable isotope labeling by amino acids in cell culture, SILAC) was performed in proliferating myoblasts 48 h after infection with adeno-ShRNA against Zc3h10 (day 0, Fig EV3A; knockdown shown in Fig EV4A). We silenced Zc3h10 in proliferating myoblasts to capture molecular pathways affected by Zc3h10 knockdown that might be driving the subsequent phenotype, rather than simply being a reflection of them. Silencing of Zc3h10 resulted in 137 upregulated and 170 downregulated proteins from a total of 3,712 identified (Fig EV4B and Dataset EV1). Gene ontology (GO) analysis detected significant enrichment of biological processes only for downregulated proteins; enriched processes included ETC, iron ion transport, and mRNA metabolic process (Fig EV4C). SILAC analysis also revealed that protein levels of subunits of complex I (Ndufa7, Ndufa8, and Nudfb10), complex III (Uqcrb and Uqcrq), complex IV (Cox5a), and mtDNA-encoded Co2 and Atp8 were notably decreased in Zc3h10 knockdown myoblasts (Fig EV4D). To assess the extent to which changes in protein expression evoked by Zc3h10 knockdown in proliferating myoblasts 48 h after infection altered levels of cellular metabolites, we used targeted metabolomics. Steady-state measurements indicated that Zc3h10 silencing increased AMP and ADP and concomitantly decreased ATP and NADH levels (Fig 5A). These latter data are consistent with SILAC findings showing reduced levels of some subunits of the Oxphos. Interestingly, Zc3h10-silenced cells also had reduced levels of pyruvate, α-ketoglutarate (α-KG), fumarate, malate, and oxaloacetate (OAA), and increased levels of succinate (Fig 5A).

To gain more detailed insight into mitochondrial substrate utilization, we cultured myoblasts in the presence of [U-$^{13}C_6$]glucose, [U-$^{13}C_{16}$]palmitate, or [U-$^{13}C_5$]glutamine for 6 h. These analyses showed that palmitate and glucose utilization, based on acetyl-CoA mole percent enrichment (MPE) and M2 levels, were not affected in Zc3h10-silenced cells (Fig 5B, C, E, and F). However, glucose-derived α-KG MPE and palmitate-derived fumarate MPE were decreased relative to scramble control cells (Fig 5B and C). In addition, we observed higher levels of glutamine-derived α-KG MPE in Zc3h10-depleted cells (Fig 5D). Isotopic enrichment was used to provide further insight into tricarboxylic acid (TCA) cycle activity. We found reduced levels of glucose-derived M2 α-KG, M2 malate and M4 succinyl-CoA (Fig 5E), and of palmitate-derived M3 and M4 fumarate and M3 OAA in Zc3h10-silenced cells (Fig 5F). Glutamine oxidative metabolism was also reduced, as evidenced from decreased M4 malate and M4 citrate (Fig 5G, green bars). Together, these results indicate slower TCA cycle flux in Zc3h10-silenced cells. Instead, glutamine reductive pathway was increased following Zc3h10 knockdown as evidenced from M5 and M2 citrate, M3 malate, M2 and M4 OAA, and M2 and M4 α-KG (Fig 5G, light green bars). Importantly, expression of TCA cycle enzymes was not significantly altered in Zc3h10-depleted cells (Fig EV4E). In sum, these data show that a primary effect of Zc3h10 depletion is a reduction in electron transport chain (ETC) activity that, in turn, negatively impacts TCA cycle function (Fig 5H).

A mutation in Zc3h10 is associated with metabolic abnormalities and mitochondrial dysfunction in humans

We next sought to ascertain whether our findings in mouse cells would translate to human pathophysiology. We examined the human Zc3h10 gene and found a single nucleotide polymorphism (SNP) in the coding sequence, an A/G non-synonymous SNP (rs61732294) at codon 105 (Fig 6A). This nucleotide substitution converts tyrosine (Tyr; Y) 105 into cysteine (Cys; C) (Fig 6A). We used PolyPhen-2 [22] to predict the impact of this amino acid substitution on the structure and function of Zc3h10 and found that Tyr105 to Cys105 exchange is likely damaging, with a score of 1 on a scale from 0 (no damage) to 1 (damaging mutation) (Fig EV5A). Zc3h10 is 97% conserved between mouse and human and Tyr105 is completely conserved across all vertebrate species examined (Fig EV5B), suggesting a critical function for this tyrosine. To examine the impact of this mutation on human physiology, we genotyped 1,594 subjects from the Progressione della Lesione Intimale Carotidea (PLIC) study [23–26] for the rs61732294 SNP and found four subjects homozygous for the mutant Cys105 allele. Remarkably, Zc3h10 Cys105 homozygotes displayed considerably higher body mass index (BMI), waist circumference, total fat mass, waist to hip ratio, fasting glucose, and triglyceride levels relative to Tyr105 carriers (Fig 6B and Table EV1). Cys105 homozygotes also had decreased HDL levels (Table EV1). These findings show that this mutation in Zc3h10 is associated with deleterious metabolic traits in humans.

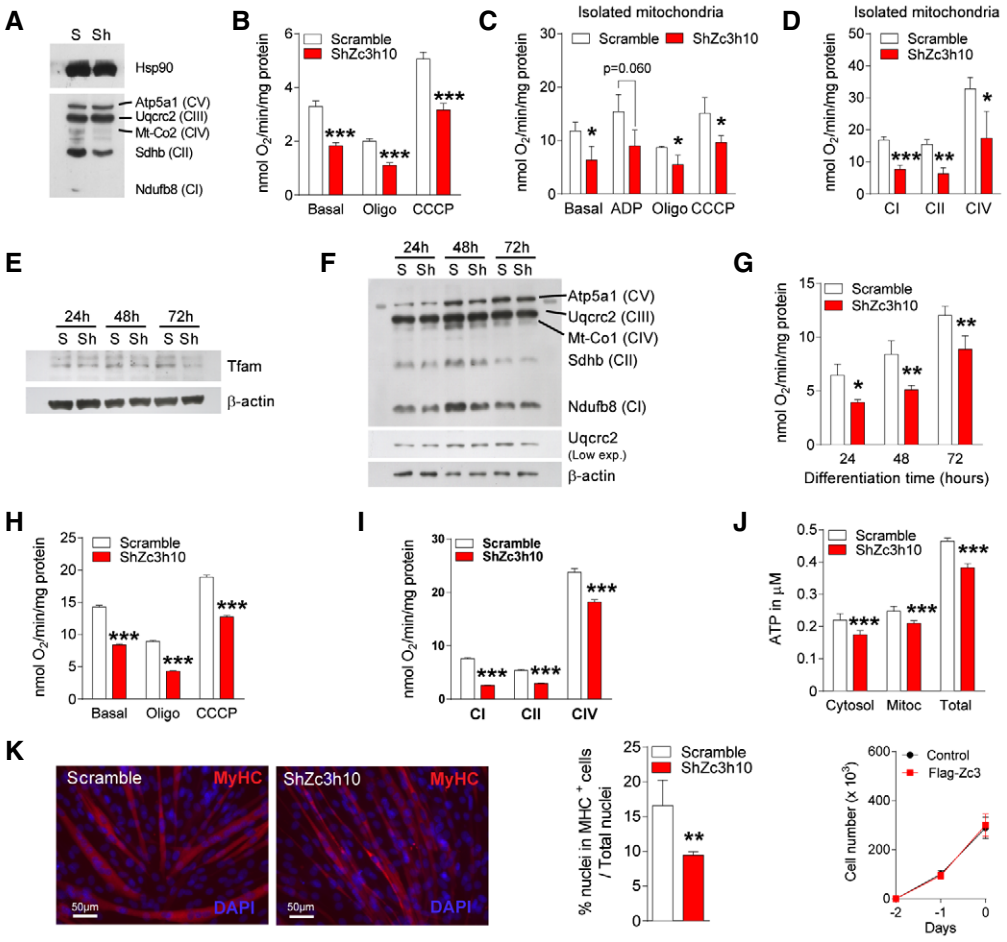

Figure 4. Impaired mitochondrial function in Zc3h10-silenced C2C12 myoblasts and myotubes.

A Western blot analysis to assess expression levels of indicated OXPHOS subunits in C2C12 myoblasts expressing scramble or Zc3h10 shRNA.

B Basal, uncoupled, and maximal uncoupled respiration in C2C12 myoblasts 48 h after infection with scramble or Zc3h10 shRNA. $n = 3$. Statistical analysis was performed by Student's *t*-test; $^{***}P < 0.001$ vs. scramble.

C, D Basal, maximal coupled, uncoupled, and maximal uncoupled respiration (C), and complex I, II, and IV activities (D) in mitochondria isolated from C2C12 myoblasts expressing scramble or Zc3h10 shRNA. $n = 3$. Statistical analysis was performed by Student's *t*-test. $^{*}P < 0.05$, $^{**}P < 0.01$, $^{***}P < 0.001$ vs. scramble.

E–G Tfam (E) and indicated Oxphos subunit (F) protein levels and (G) basal oxygen consumption in scramble and shZc3h10 myotubes 24, 48, and 72 h after induction of differentiation. $n = 3$. Statistical analysis was performed by two-way ANOVA with Sidak post-test. $^{*}P < 0.05$, $^{**}P < 0.01$ vs. scramble.

H–J Basal, uncoupled, and maximal uncoupled respiration (H); complex I, II, and IV activities (I); and cytosolic, mitochondrial, and total ATP levels (J) in scramble and Zc3h10 shRNA C2C12 myoblasts. (H) and (I) $n = 3$, (J) $n = 4$. Statistical analysis was performed by Student's *t*-test. $^{***}P < 0.001$ vs. scramble.

K Myotube fusion index 72 h after induction of differentiation with relative quantification, and myoblast proliferation rate of scramble and shZc3h10 expressing C2C12 myotubes. Fusion index, $n = 4$; proliferation, $n = 3$. Statistical analysis was performed by Student's *t*-test. $^{**}P < 0.01$ vs. scramble.

Data information: *n* indicates the number of biological replicates. Data are expressed as mean ± SD, and *P*-values were calculated from the indicated *n* independent experiments according to [44].

In support of this notion, we found that, in contrast to the effect elicited by the wild-type Tyr105 form, overexpression of Zc3h10 Cys105 in C2C12 myoblasts did not significantly increase Tfam promoter activity (Figs 7A and EV5C). Furthermore, overexpression of Cys105 Zc3h10 in C2C12 myoblasts (day 0) had no effect on basal, maximal coupled, uncoupled, or maximal uncoupled respiration, or on ETC complex activities (Fig 7B).

To examine whether the Zc3h10 Cys105 mutation in humans results in similar phenotypes to those observed in mouse cells, namely mitochondrial dysfunction, we obtained peripheral blood mononuclear cells (PBMCs) from two consented Zc3h10 Cys105 homozygous subjects (males, 75 and 57 years old) and four age-matched controls (males, 68, 74, 76, and 55 years old). Zc3h10 is expressed well in PBMCs [27]. We measured basal, maximal coupled, uncoupled, maximal uncoupled respiration, and complex I and II activities in PBMCs from homozygote Cys105 subjects and found that all these parameters were dramatically decreased (Fig 7C). Expression of Tfam, Sdhb, and Ndufb8 was also reduced (Fig 7D and E). Furthermore, steady-state metabolomics revealed that key metabolites of the TCA cycle were significantly reduced in Cys105 homozygous subjects (Fig 7F).

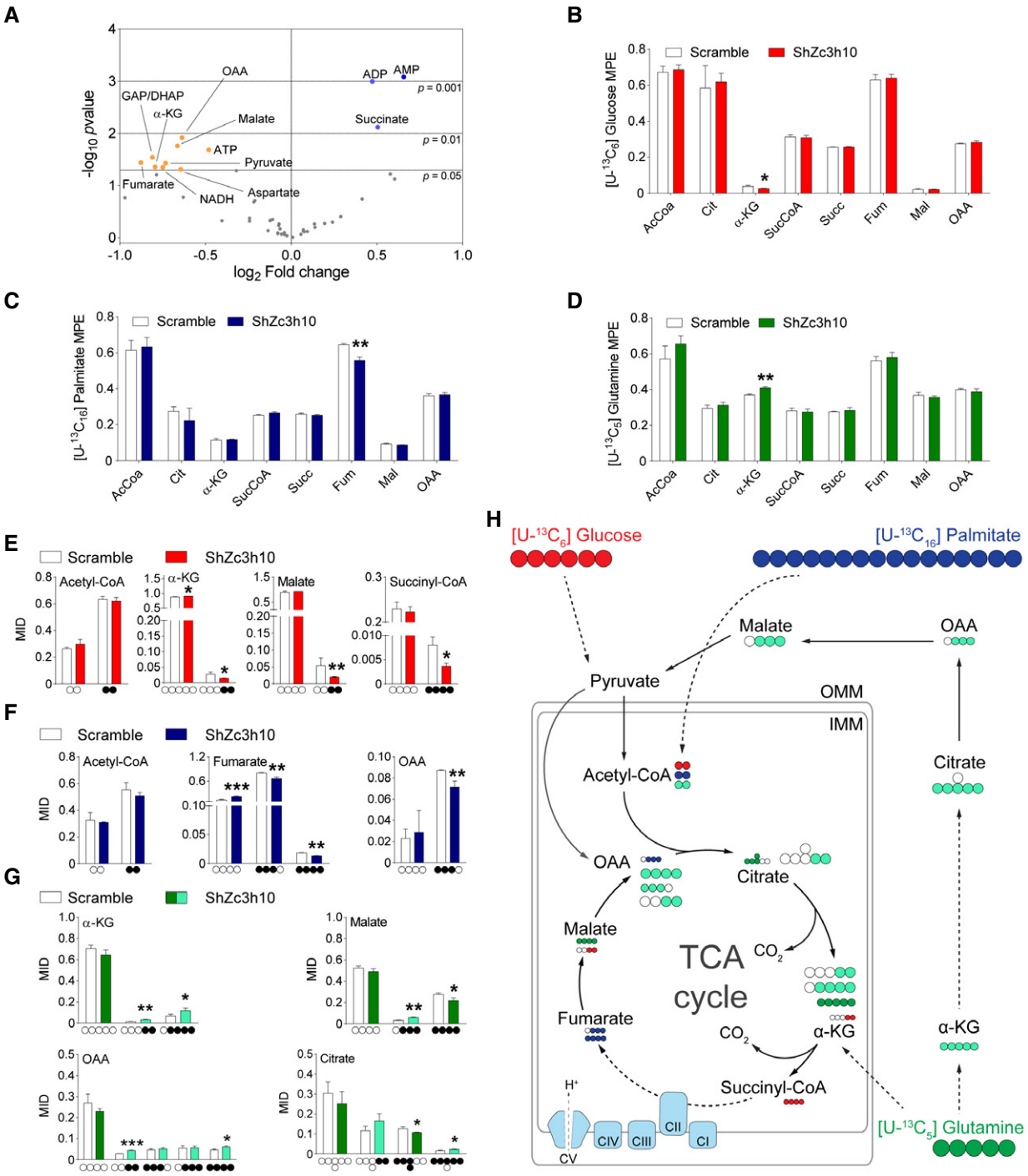

Figure 5. Zc3h10 depletion alters the ETC and rewires energy metabolism.

A Volcano plot of differentially regulated metabolites in myoblasts 48 h after infection with scramble or Zc3h10 shRNA. Analysis was performed by targeted LC-MS/MS. $n = 5$. Statistical analysis was performed by Student's t-test vs. scramble. Statistical significance is indicated in the plot.

B–G Mole percent enrichment (MPE) and mass isotopomer distribution (MID) of indicated metabolites labeled with (B, E) [U-$^{13}C_6$] glucose (red), (C, F) [U-$^{13}C_{16}$] palmitate (blue), and (D, G) [U-$^{13}C_5$] glutamine (green) in scramble and ShZc3h10 myoblasts. Light green bars indicate reductive glutamine metabolism. $n = 3$. Statistical analysis was performed by Student's t-test. $^*P < 0.05$, $^{**}P < 0.01$, $^{***}P < 0.001$ vs. scramble.

H Schematic representation of nutrient carbons flow through the TCA cycle. Large and small circles represent increased and decreased metabolites, respectively. Carbons derived from [U-$^{13}C_6$] glucose are indicated as red circles, [U-$^{13}C_{16}$] palmitate as blue circles, and [U-$^{13}C_5$] glutamine as green and light green circles indicating oxidative and reductive glutamine metabolism, respectively.

Data information: n indicates the number of biological replicates. Data are expressed as mean ± SD, and P-values were calculated from the indicated n independent experiments according to [44].

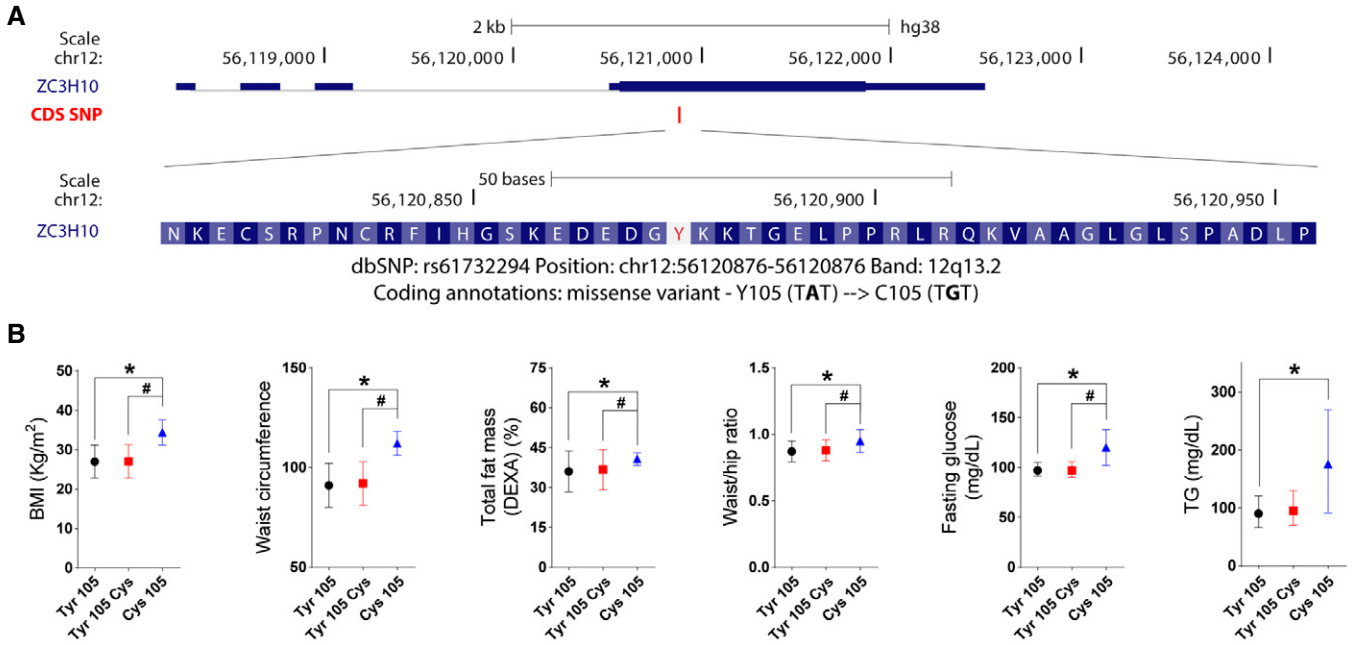

Figure 6. Tyr105 to Cys105 point mutation in human ZC3H10 is associated with altered metabolic phenotype.

A Genome browser representation of Hg38 ZC3H10 locus (upper part) and sequence of the tyrosine 105 (red) neighborhood in ZC3H10 coding sequence (lower part).

B Body mass index (BMI), waist circumference, total fat mass, waist/hip ratio, fasting glucose and triglyceride (TG) in Tyr105 (black), Tyr105Cys (red), and Cys105 (blue) subjects. Tyr105, n = 697. Tyr105Cys, n = 893. 105Cys, n = 4. Data are expressed as mean ± SD for BMI, waist circumference, total fat mass, and waist/hip ratio. For fasting glucose and TG, data are expressed as median ± interquartile range (Tyr105 and Tyr105 Cys) and mean ± SD for Cys105. Statistical analysis was performed by Kruskal–Wallis (Dunn's *post hoc* analysis). $^{*}P < 0.05$ vs. Tyr105 and $^{\#}P < 0.05$ vs. Tyr105Cys.

Together, these findings indicate that the rs61732294 SNP in human Zc3h10 (Tyr105 to Cys105) is a loss-of-function mutation that negatively impacts mitochondrial activity.

Discussion

Alterations in mitochondrial function are a driving feature in the pathogenesis of multiple human diseases, from metabolic dysfunction to neurodegeneration, yet knowledge of the molecular mechanisms that control mitochondria number and function remains incomplete [28]. Multifaceted approaches can facilitate the discovery of new regulators of mitochondria [29,30]. In this study, we used a genome-wide cDNA overexpression screen followed by assays of mitochondrial number and activity to identify the poorly characterized protein Zc3h10 as a new regulator of mitochondrial physiology. Using integrated multidisciplinary approaches, we demonstrate that Zc3h10 resides in the nucleus and it is required for the proper functioning of this organelle. Depletion of Zc3h10 in mouse cells, or a loss-of-function mutation (Tyr105Cys) in humans, results in reduced respiratory capacity and impairment of mitochondrial metabolic pathways. The slower flow of nutrient carbons into the TCA cycle, impaired respiration as result of reduced ETC complex activity, and deficient ATP production we have documented in Zc3h10 knockdown cells or human Tyr105Cys homozygotes supports the notion that Zc3h10 represents a mitochondrial regulator. Furthermore, human homozygotes for this Zc3h10 mutation have increased BMI, fat mass, altered fat distribution, elevated circulating triglyceride and glucose levels, and decreased plasma HDL, all traits that corroborate the importance of this poorly characterized protein in human physiology.

Zinc finger domains confer to proteins the ability to interact with nucleic acids, especially DNA. However, members of the CCCH (Cys-Cys-Cys-His) zinc finger family have been shown to bind to RNA and to be involved in RNA metabolism [31]. Zc3h10 contains three different CCCH motifs, a glycine-rich domain at the N-terminus, and a proline-rich motif at the C-terminus [32]. It has been described as an RNA binding protein (RBP) that can bind mRNA in Hela cells [33], 7-mer synthetic RNAs [34], and microRNA in various cell lines [35]. As regards the biological processes, it has also been reported to behave as a tumor suppressor in MCF-7 cells [36].

Other RBPs have been described that modulate the levels of mitochondrial proteins and consequently mitochondrial function. In mammals, Clu1/CluA homologue (CLUH) has been shown to be an RBP that binds a subset of mRNAs of nuclear-encoded mitochondrial proteins. However, CLUH is cytoplasmic and its action is restricted to this compartment [37]. Similarly, Puf3p, and members of the Puf or Pumilio family of RBPs in yeast, bind mRNAs that encode mitochondrial proteins, but do so nearly exclusively in the cytoplasm [38]. In addition, several mitochondrial RBPs have been identified [29,39–43]. However, to the best of our knowledge, Zc3h10 is the first mammalian RBP that resides in the nucleus and, by a currently unknown mechanism, regulates mitochondrial function.

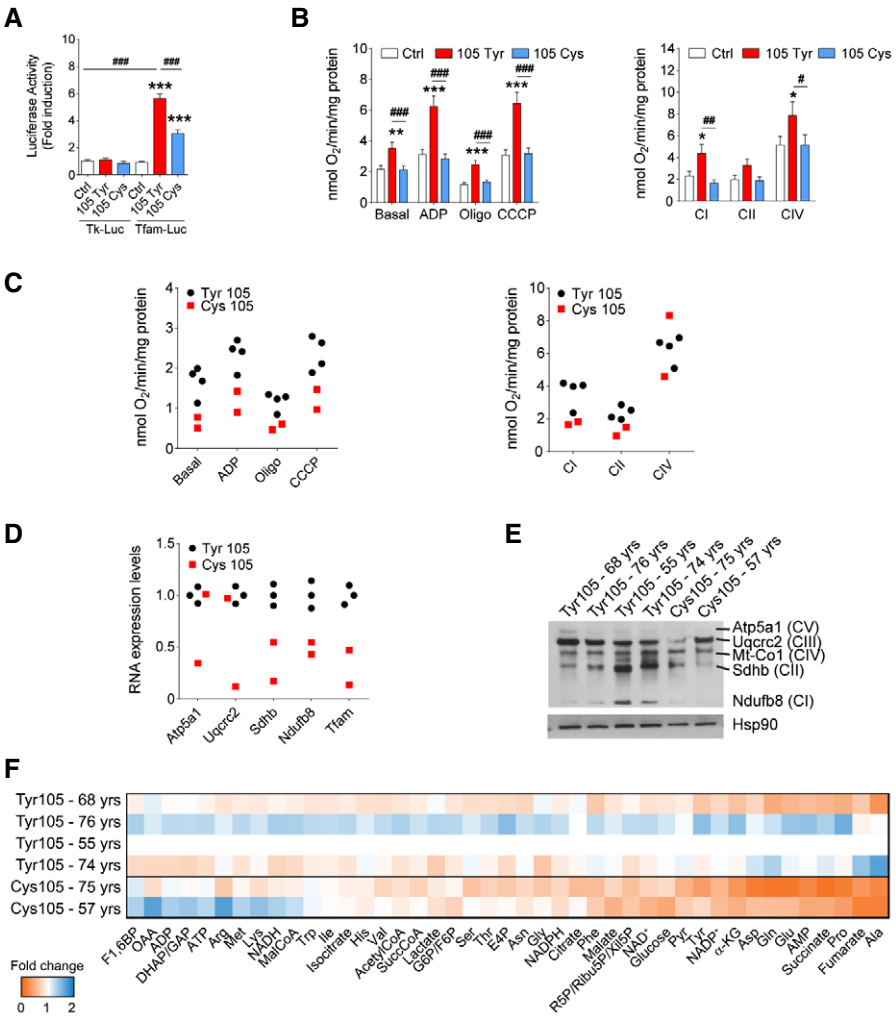

Figure 7. Loss-of-function mutation in Zc3h10 is associated with mitochondrial dysfunction in humans.

A Myoblasts were co-transfected with control, wild-type mouse Zc3h10, or Cys105 mouse Zc3h10 mutant and the indicated reporter constructs. Luciferase activity was measured 48 h later. $n = 4$. Data are expressed as mean ± SD. Statistical analysis was performed by one-way ANOVA with Dunnett's post-test. $^{***}P < 0.001$ vs. Tfam-Luc control and $^{\#\#\#}P < 0.001$ vs. Tfam-Luc Tyr105 wild-type Zc3h10.

B Basal, maximal coupled, uncoupled, maximal uncoupled respiration, and ETC complex I, II, and IV activities in C2C12 myoblasts transfected with wild-type or Cys105 Zc3h10. $n = 3$. Statistical analysis was performed by one-way ANOVA with Tukey's post-test. $^{*}P < 0.05$, $^{**}P < 0.01$, $^{***}P < 0.001$ vs. control and $^{\#}P < 0.05$, $^{\#\#}P < 0.01$, $^{\#\#\#}P < 0.001$ vs. wild-type Zc3h10.

C Basal, maximal coupled, uncoupled, and maximal uncoupled respiration, and complex I, II, and IV activities in isolated human peripheral blood mononuclear cells (PBMCs) of controls and Zc3h10 Cys105 homozygotes.

D *Tfam*, *Atp5a1*, *Uqcrc2*, *Sdhb*, and *Ndufb8* mRNA levels in PBMCs isolated from Tyr105 and Cys105 homozygote subjects.

E Western blot showing Atp5a1, Uqcrc2, Mt-CO1, Sdhb, and Ndufb8 protein expression levels in PBMCs isolated from indicated subjects.

F Heatmap of targeted metabolomics in PBMCs isolated from Tyr105 and Cys105 homozygote subjects. Blue and orange squares show increased and decreased metabolites, respectively.

Data information: *n* indicates the number of biological replicates. Data are expressed as mean ± SD, and *P*-values were calculated from the indicated *n* independent experiments according to [44].

A critical role for Zc3h10 in mitochondrial function is supported by its wide expression among mammalian tissues and the prominent degree of conservation among vertebrates, and of Tyr105 in particular, which intimates that the molecular mechanisms this protein regulates likely exist across mammals and tissues. This notion is further sustained by our identification of a loss-of-function mutation (Tyr105Cys) in humans that results in compromised mitochondrial function in PBMCs. Homozygote Cys105 cells display decreased oxygen consumption, altered ETC activity, reduced expression of some mitochondria-related genes, and an altered energetic metabolomic profile, all overt features of dysfunctional mitochondria.

In closing, we note the power of functional genomics and of integrated multidisciplinary approaches to gain insight into the molecular pathways that regulate mitochondrial biology, for, as we have shown, proteins of clear physiologic relevance in humans can be identified and characterized.

Materials and Methods

Human samples

Human quadriceps were obtained from the Telethon Tissue Bank. Specifically, male samples (n = 3) were Caucasian 67-, 76-, and 71-year-old subjects. Female samples (n = 4) were Caucasian 72-, 78-, 74-, and 67-year-old subjects. Samples were processed for RNA extraction as described below. Genotyping for the Tyr105Cys missense mutation (rs61732294) on the ZC3H10 locus was available on 1,594 Caucasian subjects; 697 wild-type allele (A) carriers, 893 heterozygous, and four homozygous for the rare mutated allele (G) were found. Subjects were obtained from The Progressione della Lesione Intimale Carotidea (PLIC) Study (a sub-study of the CHECK study), a large survey of the general population of the northern area of Milan (n = 2.606), followed at the Center for the Study of Atherosclerosis, Bassini Hospital (Cinisello Balsamo, Milan, Italy). The study was approved by the Scientific Committee of the Università degli Studi di Milano (Cholesterol and Health: Education, Control and Knowledge—Studio CHECK (SEFAP/Pr.0003)—reference number Fa-04-Feb-01) in February 4, 2001 and performed in accordance with the Declaration of Helsinki. All participants singed the informed consent. Skeletal muscle mass (SMM) was derived from Hansen formula: 1.333*(FFSTarms + FFSTlegs). The sum of FFST (fat-free soft tissue) in the arms and legs is assumed as the limb SMM, primarily reflecting 75% of total limb weight [45]. Genomic DNA was extracted using the FlexiGene DNA kit (Qiagen) as previously described [46], and genotyping was performed by TaqMan-based allelic discrimination test, using a commercial TaqMan SNP genotyping assay for rs61732294 (Thermo Fisher Scientific).

For PBMCs isolation, 30 ml of blood (supplemented with EDTA) was split in two tubes of 15 ml and spin for 12 min at 1,000 *g*. Plasma was discarded, and the interface between plasma and red blood cells, enriched in leukocytes and platelets, was carefully collected, diluted with PBS, and stratified on 3 ml of Ficoll-PlaqueTM PREMIUM (GE-Healthcare 17-5442-03). After centrifugation of 35 min at 250 *g*, PBMCs layer was carefully collected and was washed three times with 10 ml of cold PBS at 180 *g* for 12 min to get rid of platelets.

Mouse studies

Two-month-old male C57BL6/J mice were purchased from Charles River (USA) and sacrificed fed *ad libitum* after 2 weeks of maintenance for tissue collection. All experiments were conducted following the ARRIVE guidelines and regulations of the European Community (EU Directive 2010/663/EU, Official Journal of the European Union L 276/33, 20/10/2010) and local regulations (Italian Legislative Decree n. 26—04/03/2014) for the care and use of laboratory animals. The Italian Ministry of Health approved the animal protocols of this study (ministerial decree n. 579/2015-PR).

Cell lines

HEK293 (ATCC, CRL-1573) and C2C12 myoblasts (ATCC, CRL-1772) were maintained in growth medium (high-glucose DMEM supplemented with 10% fetal bovine serum (FBS) (v/v) (Gibco), 2% glutamine (v/v) (Thermo Fisher Scientific), 2% pen/strep (v/v) (Thermo Fisher Scientific) and in 37°C, 5% CO_2 and 90% humidified atmosphere). C2C12 myoblasts were differentiated to myotubes by growing cells to complete confluence and switching growth medium to differentiation medium (2% horse serum (v/v) (Euroclone), 2% glutamine (v/v), 2% pen/strep (v/v)). For metabolic labeling, C2C12 myoblasts were grown in Heavy and Light SILAC media prepared adding to the SILAC DMEM (M-Medical, FA30E15086), depleted of lysine and arginine, 10% dialyzed FBS (Invitrogen, 26400-044), 1% glutamine, 1% Pen/Strep, 10 mM HEPES pH 7.5, and either the light isotope-coded amino acids $^{12}C_6{}^{14}N_2$ L-lysine (Lys 0) and $^{12}C_6{}^{14}N_4$ L-arginine (Arg0) or their heavy isotope-counterparts: $^{13}C_6{}^{15}N_2$ L-lysine (Lys 8, Sigma-Aldrich, 68041) and $^{13}C_6{}^{15}N_4$ L-arginine (Arg10, Sigma-Aldrich, 608033). Lys and Arg were added at a concentration of 146 and 84 mg/l, respectively, light-labeled and heavy-labeled myoblasts were seeded in a 6-well plate after reaching complete incorporation.

Genomic overexpression screens

High-throughput primary screen

The mammalian gene collection (MGC) v2 library contains roughly 16,000 fully sequenced cDNAs from mouse and human genome. The library was arrayed in 384-well format containing 40 ng of cDNA per well. Each well was incubated with 20 μl of serum-free medium containing Fugene6 (Roche, 11815075001) and indicated reporter plasmid, for about 20 min. Approximately 40 ng per well of Tfam luciferase reporter system was used. The human Tfam promoter was cloned into pTK-luc in *HindIII* and *BamHI* restriction sites using the same strategy described by Virbasius and Scarpulla [47]; 8,000 trypsinized cells (human embryonic kidney (HEK293) were delivered to wells in 20 μl of serum-containing medium, and then, 384-well plates were placed in a humidified incubator (5% CO_2, 37°C). After 48 h, 40 μl of the luciferase assay reagent Bright-Glo (Promega) was added to each well, and luminescence was read within 10 min using an Acquest Plate Reader (LJL Biosystems, Sunnyvale, CA). Library was run in duplicate. All fluid delivery was done by using Multidrop (Titertek, Huntsville, AL). Relative light activity was normalized on a per-plate basis, and hits were ranked according to median activation. Positive (Pgc-1α) and negative (Mybbp1a) controls as pcDNA3 as empty control were present in each plate.

Secondary screen

The 440 hits were overexpressed, in duplicate, in HEK293 cells with the same protocol used in primary screening and 48 h after transfection were stained with both Mitotracker® Green and Mitotracker® Red CM-H_2XRos (200 nM, Thermo Fisher Scientific). Cells were trypsinized and suspended in phosphate buffer for FACS analyses using 384-well plate BD FACSCalibur™ (BD Bioscience) equipped with FlowJo software (FlowJo, LLC).

Tertiary screen

The 20 prioritized hits were overexpressed by retro-transfection of 6.25 μg of each single cDNA including also pcDNA3 as empty vector and Pgc-1α as positive controls. cDNAs were incubated with Fugene6 (Roche, 11814443001) at 1:5 μg/μl ratio in 50 μl of DMEM antibiotics and serum free. After 30 min, ~500,000 cells were added

to mixture, incubated for 40 min at room temperature, and plated in 6-well black plates. After 48 h from transfection, mitochondrial (mt) DNA content and oxygen consumption were evaluated as described below.

C2C12 myoblast transfection

C2C12 myoblasts were retro-transfected with 1.25 μg of cDNA (pcDNA3 empty vector, Pgc-1α, and Zc3h10). cDNAs were incubated with Fugene6 (Roche, 11814443001) at 1:5 μg of DNA/μl ratio in 50 μl of DMEM antibiotics and serum free. After 30 min, ~200,000 cells were added to mixture, incubated for 40 min at room temperature, and plated in 6-well plates. Co-transfection of pcDNA3 empty vector, Pgc-1α, and Zc3h10 with pTK-luc or pTK-Tfam promoter-luc plasmids was performed using 1.5 μg of total DNA (0.9 μg of cDNA and 0.6 μg of reporter plasmid) incubated with Fugene6 (Roche, 11814443001) at 1:5 μg of DNA/μl ratio in 45 μl of DMEM antibiotics and serum free. After 30 min, ~200,000 cells were added to mixture and incubated for 40 min at room temperature. The mixture was diluted with DMEM in order to seed 20,000 cells/well in 96-well plates. The same protocol was used for Zc3h10 Cys105 mutant experiments (Zc3h10 Cys105 obtained from Eurofins Genomics).

Tfam promoter activity assay

Tfam promoter or pTK-luc activity was analyzed 48 h after co-transfection of C2C12 myoblasts in 96-well plates. We removed medium and washed cells once with PBS. We then added 50 μl of fresh Britelite (Perkin Elmer) solution prepared according to manufacturer's instructions and incubated 2 min before measuring luminescence intensity in an EnVision plate reader (Perkin Elmer).

Cell transduction for gene overexpression and downregulation

Zc3h10 overexpression in C2C12 myoblasts was performed by exposing cells to adenoviral vectors for 48 h (Human Adenovirus Type 5 dE1/dE3). Validated adenoviral vector carried mouse Zc3h10 cDNA fused together with a Flag-tag to the N-terminal portion (Flag-Zc3h10) controlled by a CMV promoter (Vector Biolabs, ADV-276549). As control, we used the same construct expressing the GFP under the control of CMV promoter (Vector Biolabs, 1768). Flag-Zc3h10 and GFP were overexpressed at a multiplicity of infection (MOI) of 5. Zc3h10 targeted silencing in C2C12 myoblasts was carried out by 48 h exposure. Validated adenoviral construct contained specific short hairpin RNA sequence under a U6 promoter (shADV-276549), while control vector contained a scrambled sequence (Vector Biolabs, 1122).

Total DNA and mitochondrial DNA quantification

Total genomic and mtDNA were isolated using genomic DNA from tissues kit (Macherey-Nagel, 740952.250). Briefly, samples were scraped from dishes and spun at 1,000 *g* for 3 min at 4°C. Cells were then lysed, and DNA was isolated following manufacturer's instructions. Samples were eluted in 50 μl of DNase and RNase-free water and quantified by UV spectrophotometry (NanoDrop 1000 Spectrophotometer, Thermo Fisher Scientific). Mitochondrial DNA content was evaluated by assessing mt-Co2 and 36B4 content as mitochondrial and nuclear-encoded genes, respectively. Primers and probes were obtained from Eurofins Genomics MWG Operon and are available upon request.

Gene expression analysis

Total RNA was obtained from C2C12, PBMCs, and different mouse tissues and human quadriceps using a commercial kit (NucleoSpin® RNA extraction kit, Macherey-Nagel, 740955.250). Briefly, cells were washed in ice-cold PBS and lysed in 350 of lysis buffer supplemented with 1% β-mercaptoethanol. Mouse tissues and human quadriceps were transferred to 400 μl of PureZOL (Bio-rad, 732-6890) and lysed using tissue lyser at highest frequency for 3 min. After adding 100 μl of chloroform, mouse samples were centrifuged at 10,000 *g* at 4°C for 15 min. Upper polar phases and cell samples were then transferred to columns and spun 11,000 *g* for 30 s. Total RNA was then isolated by following manufacturer's instructions and eluted from columns with 50 μl of RNase-free water. Total RNA amount was then quantified by UV spectrophotometry (NanoDrop 1000 Spectrophotometer, Thermo Fisher Scientific). Samples were then diluted to 5 ng/μl and used for mRNA quantification. RNA was quantitated by qRT–PCR using iScriptTM One Step for Probes (Bio-rad, 1725141) and iTaq Universal SYBR Green One-Step Kit for qPCR (Bio-rad, 1725151), following the manufacturer's instructions. The qRT–PCR protocol is composed of 40 cycles of amplifications, each consisting of a denaturation step at 95°C for 15 s and an annealing/extension step at 60°C for 60 s. The oligonucleotides used for qRT–PCR were obtained from Eurofins MWG Operon (Ebersberg, Germany). qRT–PCR primers sequences are available in Table EV2.

Microarray analysis

Microarray analysis for whole transcriptome analysis was performed using a MoGene 2.0 chip. Briefly, C2C12 myotubes were differentiated for 2 days. Cells were then rinsed in 1 ml of ice-cold PBS. Total RNA was isolated as described above, and 3 μg of RNA was used for following analyses. Total RNA concentration and purity was assessed by UV spectrophotometry (NanoDrop 1000 Spectrophotometer, Thermo Fisher Scientific). Total RNA integrity was assessed by Agilent Bioanalyzer, and the RNA Integrity Number (RIN) was calculated before differential gene expression evaluation. C2C12 RNA was analyzed by the Genopolis Consortium (Italy) using an Affimetrix platform.

Mass spectrometry (MS)-based expression proteomics

SILAC labeling of cells and sample preparation prior to LC-MS/MS

Light cells were infected with scramble shRNA, while heavy cells were infected with Zc3h10 shRNA and exposed to adenoviral vectors for 48 h. Proteins from both conditions were extracted in RIPA buffer (15 mM NaCl, 0.1% NP-40, 0.05% Na-deoxycholate, 5 mM Tris–HCl pH 8.0), quantified using Bradford assay, and mixed in 1:1 ratio. Protein lysates were separated by SDS–PAGE on a gradient gel (4–12% Tris–HCl Precast Gel, Invitrogen) and stained with Colloidal Coomassie. Enzymatic in-gel digestion of proteins with trypsin protease was performed essentially as previously described

[48]. Briefly, samples were subjected to reduction in DTT 10 mM for 1 h at 56°C, followed by alkylation with iodoacetamide 55 mM for 45 min at RT, in the dark. Digestion was carried out saturating the gel with sequencing-grade, modified trypsin 12.5 ng/ml (Promega) in ammonium bicarbonate 50 mM, O/N. Peptide mixtures were acidified with tri-fluoro acetic acid (TFA, final concentration 3%), extracted from gel slices with two rounds of washes (in 30% acetonitrile (ACN)/3% TFA and then in 100% ACN, respectively), and concentrated to ~5 μl in a vacuum concentrator (Eppendorf). Samples were loaded onto home-made C18-Stage Tips, for concentration and desalting prior LC-MS/MS analysis [49].

Liquid chromatography and tandem mass spectrometry (LC-MS/MS)

Peptide mixtures were analyzed by online nano-flow LC-MS/MS using an EASY-nLC 1000 (Thermo Fisher Scientic) connected to a QExactive (Thermo Fisher Scientific) through a nanoelectrospray ion source. The nano-LC system was operated in one column setup with a 25-cm analytical column (75 μm inner diameter, 350 μm outer diameter) packed with C18 resin (ReproSil, Pur C18AQ 1.9 m, Dr. Maisch, Germany) configuration. Solvent A was 0.1% formic acid (FA) in ddH_2O, and solvent B was 80% ACN with 0.1% FA. Samples were injected in an aqueous 1% FA solution at a flow rate of 500 nl/min. Peptides were separated with a gradient of 5–30% solvent B for 90 min, followed by a gradient of 30–60% in 5 min, and 60–95% over 5 min at a flow rate of 250 nl/min. The QExactive instrument was operated in the data-dependent acquisition (DDA) to automatically switch between full scan MS and MS/MS acquisition. The MS spectra (from m/z 375–1650) were analyzed in the Orbitrap detector at resolution of 60 000 (200 m/z). The fifteen most intense peptide ions were sequentially isolated to a target value of 3 × 106 and fragmented by HCD with a normalized collision energy setting of 27%. The maximum allowed ion accumulation times were 20 ms for full scans and 80 ms for MS/MS, and the target value for MS/MS was set to 1 × 105 for an 15,000 of resolution at m/z 200. Standard mass spectrometric conditions for all experiments were as follows: spray voltage, 2.1 kV; no sheath and auxiliary gas flow.

Analysis of proteomics data

The mass spectrometric raw data were analyzed with the MaxQuant software (version 1.5.2.8) [50]. A false discovery rate (FDR) of 1% for proteins and peptides, and a minimum peptide length of 6 amino acids were required. In order to improve mass accuracy of the precursor ions, the time-dependent recalibration algorithm of MaxQuant was used. The MS/MS spectra were searched by Andromeda engine against the UniProt mouse database (70,941 entries). Enzyme specificity was set to trypsin, and maximum of two missed cleavages were allowed. Peptide identification was based on a search with an initial mass deviation of the precursor ion of up to 7 ppm. The fragment mass tolerance was set to 20 ppm. Cysteine carbamidomethylation (Cys +57.021464 Da) was searched as fixed modification, whereas N-acetylation of protein (N-term, +42.010565 Da) and oxidized methionine (+15.994915 Da) were searched as variable modifications. SILAC peptide and protein quantification was performed automatically with MaxQuant using default settings for parameters [51]. Briefly, for each SILAC pair the ratio is determined by regression model fitted to all isotopic peaks and all pair for each scan during the peptides elution. SILAC protein ratios are determined as the median of all peptide ratios assigned to the protein. Protein ratios were transformed in $\log_2$, and the corresponding *P*-values by means of significance B were calculated by Perseus software [50,52].

Western blot

Protein relative quantification analyses were carried out by separating cell lysates on SDS–PAGE. Cells were rinsed in ice-cold PBS, centrifuged, and lysed in RIPA buffer. Protein concentration was measured using Bradford method (Bio-rad, 5000006). Proper protein amount was then loaded on 12.5% SDS–PAGE. After gel run, proteins were transferred to a nitrocellulose membrane and blocked in 5% bovine serum albumin (BSA) for 1.5 h at RT. Membranes were then incubated O/N at 4°C with primary antibodies, previously suspended in 0.1% TBS–Tween-20 and 3% BSA. After extensive washes, membranes were incubated with HRP-conjugated secondary antibodies for 1 h at RT. After washing, membranes were finally incubated with ECL substrate for bands detection. Primary and secondary antibodies were diluted as follows: Zc3h10 1:1,000 (Aviva systems biology, ARP60671_P050), Tfam 1:1,000 (Aviva systems biology, ARP31400_P050), OXPHOS cocktail 1:1,000 (Abcam, ab110413), Myosin Heavy Chain Fast (MyHCFast) 1:1,000 (Monosan, Monx10807), Hsp90 1:500 (Santa Cruz Biotech., sc-7947), β-actin 1:5,000 (Sigma-Aldrich, A5441), histone H3 1:1,000 (Millipore, 06-755), α-tubulin 1:1,000 (Sigma-Aldrich, T9026), Flag 1:5,000 (Sigma-Aldrich, F3165), α-mouse 1:5,000 (Sigma-Aldrich, A4416), and α-rabbit 1:2,000 (Cell Signaling, 7074).

Nucleus–cytoplasm separation and isolation of mitochondria

C2C12 cells were grown in complete medium and collected at different stages of differentiation for nucleus and cytoplasm protein extraction. All centrifugations were performed at 4°C, and samples were kept on ice throughout all the procedure. Cells were rinsed ice-cold PBS and suspended in 500 μl fractionation buffer (250 mM sucrose, 20 mM HEPES pH 7.4, 10 mM KCl, 2 mM $MgCl_2$, 1 mM EGTA, 1 mM EDTA, protease inhibitor, and 200 mM DTT) after centrifugation. Cell suspensions were passed through a 25-gauge needle 15 times and left in ice for 20 min. Sample was then centrifuged at 720 *g* for 5 min and saved pellet as crude nuclei fraction, while supernatant was the cytosolic fraction. Nuclear pellets were later suspended and washed with 500 μl of fractionation buffer before being passed through a 25-gauge needle other 15 times. Nuclear samples were centrifuged again at 720 *g* for 10 min, and pellet was saved as nuclear fraction. The pellet was then suspended in TBS with 0.1% SDS and sonicated 20 s at 10% to shear genomic DNA and homogenize the lysate. Finally, cytoplasmic fractions were spun at 10,000 *g* for 5 min and supernatant was saved as cytoplasmic fraction. Proteins were then quantified and equally loaded on SDS–PAGE. Mitochondria were isolated as previously described [53]. Briefly, ~50 million confluent myoblasts were washed with ice-cold PBS and harvested. They were then spun and resuspended in 1 ml of STM buffer (250 mM sucrose, 50 mM Tris–HCl pH 7.4, 5 mM $MgCl_2$, and protease inhibitor). Once resuspended, cells were passed 50 times through a 25-gauge needle and left in ice. After 30 min, cells were passed once again 50 times through a 25-gauge

and spun for 15 min at 800 *g* at 4°C. The supernatant was saved and centrifuged again 11,000 *g* for 10 min at 4°C. Crude mitochondrial fractions were resuspended in 400 μl of STM buffer and spun at 20,000 *g* for 10 min at 4°C. The pellets were considered as the pure mitochondrial fraction.

Immunofluorescence analysis

Immunofluorescence analysis was performed on 72 h differentiated myotubes. After removing the medium, cells were washed with ice-cold PBS and fixed with 1% paraformaldehyde for 15 min at RT. After three washes with Triton X-100 1% in PBS, we unmasked the antigen incubating cells with 1N HCl at 4°C for 10 min, then with 2 N HCl for 10 min and finally with 2 N HCl at 37°C for 10 min. Later, cells were treated with 0.1 M sodium borate for 10 min at RT, blocked with 2% goat serum, 1% BSA, 0.1% Tween-20, 0.05% Triton X-100 in PBS for 2 h at room temperature, and finally incubated O/N at 4°C with MyHCFast 1:250 (Monosan, Monx10807) primary antibody in PBS. After extensive washes, cells were then exposed to the goat anti-mouse Alexa Fluor 635 nm (Thermo Fisher Scientific, A-31574) secondary antibody 1:1,000 for 1 h at room temperature. After extensive ice-cold PBS washes for 30 min, cells were finally incubated with Hoechst for 10 min, washed with PBS for 5 min, and mounted on glass slides with Permafluor. Fusion index was calculated as the ratio between the number of nuclei in $MyHC^+$ fibers with three or more nuclei on total nuclei number in the field.

Metabolite extraction and LC-MS/MS analysis

Cells were grown in 6-well plates, harvested in ice-cold PBS, and centrifuged at 2,500 *g* for 3 min at 4°C. Pellets were then resuspended in 250 μl methanol/acetonitrile 1:1 containing [U-$^{13}C_6$]-Glucose-1 ng/μl (internal standard, Sigma-Aldrich, 389374) and spun at 20,000 *g* for 5 min at 4°C. Supernatant was then passed through a regenerated cellulose filter, dried, and resuspended in 100 μl of MeOH for subsequent analysis. Amino acid quantification was performed through previous derivatization. Briefly, 50 μl of 5% phenyl isothiocyanate (PITC) in 31.5% EtOH and 31.5% pyridine in water was added to 10 μl of each sample. Mixtures were then incubated with PITC solution for 20 min at RT, dried under N_2 flow, and suspended in 100 μl of 5 mM ammonium acetate in MeOH/H_2O 1:1. Metabolomic data were performed on an API-4000 triple quadrupole mass spectrometer (AB Sciex) coupled with a HPLC system (Agilent) and CTC PAL HTS autosampler (PAL System). The identity of all metabolites was confirmed using pure standards. Quantification of different metabolites was performed with a liquid chromatography/tandem mass spectrometry (LC-MS/MS) method using a C18 column (Biocrates) for amino acids and cyano-phase LUNA column (50 × 4.6 mm, 5 μm; Phenomenex) for metabolites, respectively. Methanolic samples were analyzed by a 10-min run in positive (amino acids) and 5-min run in negative (all other metabolites) ion mode with 20 multiple reaction monitoring (MRM) transition in positive ion mode and 30 MRM transition in negative ion mode, respectively. The mobile phases for positive ion mode analysis (amino acids) were phase A: 0.2% formic acid in water and phase B: 0.2% formic acid in acetonitrile. The gradient was T_0 100%A, $T_{5.5\ min.}$ 5%A, $T_{7\ min}$ 100%A with a flow rate of 500 μl/min. The mobile phase for negative ion mode analysis (all other metabolites) was phase A: 5 mM ammonium acetate pH 7.0 in MeOH. The gradient was 100%A for all the analysis with a flow rate of 500 μl/min. MultiQuant™ software (version 3.0.2) was used for data analysis and peak review of chromatograms. Quantitative evaluation of all metabolites was performed based on calibration curves with pure standards, and then, data were normalized on micrograms of DNA. For metabolic tracing analyses, confluent myoblasts were exposed for 6 h to [U-$^{13}C_6$]-glucose 1 mM (Sigma-Aldrich, 389374) or [U-$^{13}C_5$]-glutamine 2 mM (Sigma-Aldrich, 605166) or [U-$^{13}C_{16}$]-palmitate 100 μM (Sigma-Aldrich, 605573). Metabolites quantification was performed as described above by increasing the MRM transitions in negative ion mode to 139 to analyze the different isotopomers.

Oxygen consumption measurements

Oxygen consumption rate (OCR) analysis on whole cells was performed by using a Clark type oxygen electrode (Hansatech, DW1 electrode chamber). C2C12 cells were rinsed in pre-warmed PBS (37°C) and suspended in coupled respiration buffer (2% free fatty acids–BSA, 1 mM Na-pyruvate, 25 mM D-glucose, 40 μg/ml digitonin) or electron flow buffer (2% free fatty acids–BSA, 10 mM Na-pyruvate, 2 mM malate, 4 μM carbonyl cyanide m-chlorophenyl hydrazine (CCCP), digitonin 40 μg/ml). Samples were then transferred to the electrode chamber for the oxygen consumption rate measurement. After measuring basal respiration, uncoupled and maximal respiration were evaluated by adding 10 μM oligomycin and 10 μM CCCP, respectively. Complex I, II, and IV activities were evaluated through the electron flow protocol. Once transferred into the chamber, CI activity was evaluated. After 10 μM rotenone and 5 mM succinate addition, we assessed complex II activity. We then added 100 μM antimycin A and 20 mM/0.8 mM ascorbate/N,N,N′, N′-tetramethyl-p-phenylenediamine (TMPD) to measure complex IV activity. All samples values were normalized on total protein content.

150 μg of isolated mitochondria was resuspended in coupled respiration buffer (5 mM succinate, 2 mM malate, 1 mM pyruvate, 40 ng/μl digitonin, 2% free FA-BSA in PBS) or electron flow buffer (2 mM malate, 1 mM pyruvate, 40 ng/μl digitonin, 1 μM CCCP, 2% free FA-BSA in PBS). For coupled respiration, after basal measurement 10 μM ADP, 5 μM oligomycin and 5 μM CCCP were added for maximal coupled, uncoupled, and maximal uncoupled respiration, respectively. Complex I, II, and IV activities were evaluated as described above and adding 5 μM rotenone, 2.5 mM succinate, 50 μM antimycin A, and 10 mM/0.4 mM ascorbate/TMPD. All samples values were normalized on total protein content.

ATP content measurement

Cytosolic, mitochondrial, and total ATP production were analyzed 60 h after transfection or infection using a specific kit (Perkin Elmer, 6016941). Samples were exposed to DMSO or oligomycin 5 μM for 24 h. Luminescence was then analyzed to quantify cytosolic and total ATP production. Mitochondrial ATP was inferred from previous measurements, and data were normalized on total protein content.

Cell proliferation assay

Cells were seeded at a density of 2×10^5 per well and incubated in complete medium. Twenty-four hours later, cells were scraped and suspended in 10 ml of PBS or transfected with scramble or ShZc3h10 sequence. 500 µl of suspended cells was used for cell count by Z2 beck man coulter counter and considered as blank. Twenty-four and 48 h later, transduced cells proliferation was analyzed as well.

Statistical analysis

Statistical analyses were performed with Student's *t*-test, one-way ANOVA followed by Dunnett's or Tukey's post-test or two-way ANOVA followed by Sidak post-test as necessary using GraphPad Prism (version 6.0).

Data and software availability

The data discussed in this manuscript (C2C12 myotubes microarray dataset) have been deposited in NCBI's Gene Expression Omnibus [54] and are accessible through GEO Series accession number GSE99102. The mass spectrometry proteomics data have been deposited in Pride (http://www.ebi.ac.uk/pride/) with the dataset identifier PXD008833 [55].

Biogps is available at http://biogps.org/#goto=welcome, and DAVID Functional Annotation Tool is available at https://david.ncifcrf.gov/summary.jsp. Tissue set enrichment analysis (TSEA) is available at http://genetics.wustl.edu/jdlab/tsea/, while gene set enrichment analysis (GSEA) was performed to evaluate significantly enriched gen clusters in C2C12 myotubes (http://software.broadinstitute.org/gsea/index.jsp). Images quantifications were performed by ImageJ (https://imagej.nih.gov/ij/). Metabolomic mass spectrometric raw data were analyzed with the MultiQuant™ software (version 3.0.2) (https://sciex.com/products/software/multiquant-software), while proteomics raw data were analyzed with the MaxQuant software (version 1.5.2.8) (http://www.coxdocs.org/doku.php?id=maxquant:start). Prediction of ZC3H10 Tyr105Cys mutation damage was evaluated by using PolyPhen-2 software (http://genetics.bwh.harvard.edu/pph2/) [22].

Expanded View for this article is available online.

Acknowledgements
We thank F. Giavarini for his valuable help with HPLC and mass spectrometry. We also thank A. Maggi for critically reading the manuscript and for her helpful comments and all the members of the laboratory for valuable discussion. We are in debt with Ms. E. Desiderio Pinto for administrative assistance. T. Bonaldi is supported by grants from the Italian Association for Cancer Research (AIRC), the Italian Ministry of Health (RF-GR2011), and the Epigen Flagship project grant (CNR). This work is supported by Ministero della Salute GR-2011-02346974 to GDN and GR-2013-02355011 to FB; Aspire Cardiovascular Grant 2016-WI218287 to GDN, The Giovanni Armenise Harvard-Foundation Career Development Grant, Cariplo Foundation (grant number 2014-0991 to NM, 2015-0524 and 2015-0564 to ALC, 2016-0852 to GDN), European Foundation for the Study of Diabetes (EFSD)/Lilly European Diabetes Research Programme 2015 to N.M. This research was supported by grants from MIUR Progetto Eccellenza.

Author contributions
NM, ES, MA, and EDF developed the study, conceived the experiments, analyzed data, and wrote the manuscript. MA and SP performed the majority of biochemical, biological, and molecular biology experiments. DC, SP, and GC performed metabolomics analyses. EB developed methods for the analysis of selected hits. GRD and SG contributed in microarray study and to interpret data. AC carried out the acquisition and analysis of proteomic data. TB contributed to the design of SILAC experiments, supervised data analysis, and participated in the evaluation of the proteomics results. FS and MM provided and analyzed human quadriceps samples. ALC, GDN, LG, KG, AB, and FB, provided samples from the PLIC study, isolated PBMCs, and analyzed data. ES, EDF, DC, and MC analyzed data and participated in the interpretation of results. All authors read and edited the manuscript.

Conflict of interest
The authors declare that they have no conflict of interest.

References

1. Evans A, Neuman N (2016) The mighty mitochondria. *Mol Cell* 61: 641
2. Nunnari J, Suomalainen A (2012) Mitochondria: in sickness and in health. *Cell* 148: 1145 – 1159
3. Suomalainen A, Isohanni P (2010) Mitochondrial DNA depletion syndromes–many genes, common mechanisms. *Neuromuscul Disord* 20: 429 – 437
4. Schon EA, DiMauro S, Hirano M (2012) Human mitochondrial DNA: roles of inherited and somatic mutations. *Nat Rev Genet* 13: 878 – 890
5. Lowell BB, Shulman GI (2005) Mitochondrial dysfunction and type 2 diabetes. *Science* 307: 384 – 387
6. Ramadasan-Nair R, Gayathri N, Mishra S, Sunitha B, Mythri RB, Nalini A, Subbannayya Y, Harsha HC, Kolthur-Seetharam U, Srinivas Bharath MM (2013) Mitochondrial alterations and oxidative stress in an acute transient mouse model of muscle degeneration: implications for muscular dystrophy and related muscle pathologies. *J Biol Chem* 289: 485 – 509
7. Andreux PA, Houtkooper RH, Auwerx J (2013) Pharmacological approaches to restore mitochondrial function. *Nat Rev Drug Discov* 12: 465 – 483
8. Larsson NG, Wang J, Wilhelmsson H, Oldfors A, Rustin P, Lewandoski M, Barsh GS, Clayton DA (1998) Mitochondrial transcription factor A is necessary for mtDNA maintenance and embryogenesis in mice. *Nat Genet* 18: 231 – 236
9. Calvo SE, Clauser KR, Mootha VK (2016) MitoCarta2.0: an updated inventory of mammalian mitochondrial proteins. *Nucleic Acids Res* 44: D1251 – D1257
10. Kohler A, Hurt E (2007) Exporting RNA from the nucleus to the cytoplasm. *Nat Rev Mol Cell Biol* 8: 761 – 773
11. Chandel NS (2015) Evolution of mitochondria as signaling organelles. *Cell Metab* 22: 204 – 206
12. van der Knaap JA, Verrijzer CP (2016) Undercover: gene control by metabolites and metabolic enzymes. *Genes Dev* 30: 2345 – 2369
13. Su X, Wellen KE, Rabinowitz JD (2015) Metabolic control of methylation and acetylation. *Curr Opin Chem Biol* 30: 52 – 60
14. Scarpulla RC, Vega RB, Kelly DP (2012) Transcriptional integration of mitochondrial biogenesis. *Trends Endocrinol Metab* 23: 459 – 466
15. Hock MB, Kralli A (2009) Transcriptional control of mitochondrial biogenesis and function. *Annu Rev Physiol* 71: 177 – 203

16. Wu Z (1999) Mechanisms controlling mitochondrial biogenesis and respiration through the thermogenic coactivator PGC-1. *Cell* 98: 115
17. Fan M, Rhee J, St-Pierre J, Handschin C, Puigserver P, Lin J, Jaeger S, Erdjument-Bromage H, Tempst P, Spiegelman BM (2004) Suppression of mitochondrial respiration through recruitment of p160 myb binding protein to PGC-1alpha: modulation by p38 MAPK. *Genes Dev* 18: 278 – 289
18. Duguez S, Feasson L, Denis C, Freyssenet D (2002) Mitochondrial biogenesis during skeletal muscle regeneration. *Am J Physiol Endocrinol Metab* 282: E802 – E809
19. Remels AH, Langen RC, Schrauwen P, Schaart G, Schols AM, Gosker HR (2010) Regulation of mitochondrial biogenesis during myogenesis. *Mol Cell Endocrinol* 315: 113 – 120
20. Moyes CD, Mathieu-Costello OA, Tsuchiya N, Filburn C, Hansford RG (1997) Mitochondrial biogenesis during cellular differentiation. *Am J Physiol* 272: C1345 – C1351
21. Hu CJ, Wang LY, Chodosh LA, Keith B, Simon MC (2003) Differential roles of hypoxia-inducible factor 1alpha (HIF-1alpha) and HIF-2alpha in hypoxic gene regulation. *Mol Cell Biol* 23: 9361 – 9374
22. Adzhubei IA, Schmidt S, Peshkin L, Ramensky VE, Gerasimova A, Bork P, Kondrashov AS, Sunyaev SR (2010) A method and server for predicting damaging missense mutations. *Nat Methods* 7: 248 – 249
23. Norata GD, Garlaschelli K, Ongari M, Raselli S, Grigore L, Catapano AL (2006) Effects of fractalkine receptor variants on common carotid artery intima-media thickness. *Stroke* 37: 1558 – 1561
24. Norata GD, Garlaschelli K, Grigore L, Tibolla G, Raselli S, Redaelli L, Buccianti G, Catapano AL (2009) Circulating soluble receptor for advanced glycation end products is inversely associated with body mass index and waist/hip ratio in the general population. *Nutrition Metab Cardiovasc Dis* 19: 129 – 134
25. Lorenz MW, Polak JF, Kavousi M, Mathiesen EB, Volzke H, Tuomainen TP, Sander D, Plichart M, Catapano AL, Robertson CM *et al* (2012) Carotid intima-media thickness progression to predict cardiovascular events in the general population (the PROG-IMT collaborative project): a meta-analysis of individual participant data. *Lancet* 379: 2053 – 2062
26. Baragetti A, Palmen J, Garlaschelli K, Grigore L, Pellegatta F, Tragni E, Catapano AL, Humphries SE, Norata GD, Talmud PJ (2015) Telomere shortening over 6 years is associated with increased subclinical carotid vascular damage and worse cardiovascular prognosis in the general population. *J Intern Med* 277: 478 – 487
27. Su AI, Cooke MP, Ching KA, Hakak Y, Walker JR, Wiltshire T, Orth AP, Vega RG, Sapinoso LM, Moqrich A *et al* (2002) Large-scale analysis of the human and mouse transcriptomes. *Proc Natl Acad Sci USA* 99: 4465 – 4470
28. Patananan AN, Wu TH, Chiou PY, Teitell MA (2016) Modifying the mitochondrial genome. *Cell Metab* 23: 785 – 796
29. Wolf AR, Mootha VK (2014) Functional genomic analysis of human mitochondrial RNA processing. *Cell Rep* 7: 918 – 931
30. Arroyo JD, Jourdain AA, Calvo SE, Ballarano CA, Doench JG, Root DE, Mootha VK (2016) A genome-wide CRISPR death screen identifies genes essential for oxidative phosphorylation. *Cell Metab* 24: 875 – 885
31. Hall TM (2005) Multiple modes of RNA recognition by zinc finger proteins. *Curr Opin Struct Biol* 15: 367 – 373
32. Liang J, Song W, Tromp G, Kolattukudy PE, Fu M (2008) Genome-wide survey and expression profiling of CCCH-zinc finger family reveals a functional module in macrophage activation. *PLoS One* 3: e2880
33. Castello A, Fischer B, Eichelbaum K, Horos R, Beckmann BM, Strein C, Davey NE, Humphreys DT, Preiss T, Steinmetz LM *et al* (2012) Insights into RNA biology from an atlas of mammalian mRNA-binding proteins. *Cell* 149: 1393 – 1406
34. Ray D, Kazan H, Cook KB, Weirauch MT, Najafabadi HS, Li X, Gueroussov S, Albu M, Zheng H, Yang A *et al* (2013) A compendium of RNA-binding motifs for decoding gene regulation. *Nature* 499: 172 – 177
35. Treiber T, Treiber N, Plessmann U, Harlander S, Daiss JL, Eichner N, Lehmann G, Schall K, Urlaub H, Meister G (2017) A compendium of RNA-binding proteins that regulate MicroRNA biogenesis. *Mol Cell* 66: 270 – 284.e13
36. Guardiola-Serrano F, Haendeler J, Lukosz M, Sturm K, Melchner H, Altschmied J (2008) Gene trapping identifies a putative tumor suppressor and a new inducer of cell migration. *Biochem Biophys Res Commun* 376: 748 – 752
37. Gao J, Schatton D, Martinelli P, Hansen H, Pla-Martin D, Barth E, Becker C, Altmueller J, Frommolt P, Sardiello M *et al* (2014) CLUH regulates mitochondrial biogenesis by binding mRNAs of nuclear-encoded mitochondrial proteins. *J Cell Biol* 207: 213 – 223
38. Gerber AP, Herschlag D, Brown PO (2004) Extensive association of functionally and cytotopically related mRNAs with Puf family RNA-binding proteins in yeast. *PLoS Biol* 2: E79
39. Tu YT, Barrientos A (2015) The human mitochondrial DEAD-box protein DDX28 resides in RNA granules and functions in mitoribosome assembly. *Cell Rep* 10: 854 – 864
40. Jourdain AA, Koppen M, Rodley CD, Maundrell K, Gueguen N, Reynier P, Guaras AM, Enriquez JA, Anderson P, Simarro M *et al* (2015) A mitochondria-specific isoform of FASTK is present in mitochondrial RNA granules and regulates gene expression and function. *Cell Rep* 10: 1110 – 1121
41. Popow J, Alleaume AM, Curk T, Schwarzl T, Sauer S, Hentze MW (2015) FASTKD2 is an RNA-binding protein required for mitochondrial RNA processing and translation. *RNA* 21: 1873 – 1884
42. Simarro M, Gimenez-Cassina A, Kedersha N, Lazaro JB, Adelmant GO, Marto JA, Rhee K, Tisdale S, Danial N, Benarafa C *et al* (2010) Fast kinase domain-containing protein 3 is a mitochondrial protein essential for cellular respiration. *Biochem Biophys Res Commun* 401: 440 – 446
43. Antonicka H, Sasarman F, Nishimura T, Paupe V, Shoubridge EA (2013) The mitochondrial RNA-binding protein GRSF1 localizes to RNA granules and is required for posttranscriptional mitochondrial gene expression. *Cell Metab* 17: 386 – 398
44. Vaux DL, Fidler F, Cumming G (2012) Replicates and repeats–what is the difference and is it significant? A brief discussion of statistics and experimental design. *EMBO Rep* 13: 291 – 296
45. Hansen RD, Raja C, Aslani A, Smith RC, Allen BJ (1999) Determination of skeletal muscle and fat-free mass by nuclear and dual-energy X-ray absorptiometry methods in men and women aged 51–84 y (1–3). *Am J Clin Nutr* 70: 228 – 233
46. Norata GD, Ongari M, Garlaschelli K, Tibolla G, Grigore L, Raselli S, Vettoretti S, Baragetti I, Noto D, Cefalu AB *et al* (2007) Effect of the -420C/G variant of the resistin gene promoter on metabolic syndrome, obesity, myocardial infarction and kidney dysfunction. *J Intern Med* 262: 104 – 112
47. Virbasius JV, Scarpulla RC (1994) Activation of the human mitochondrial transcription factor A gene by nuclear respiratory factors: a potential regulatory link between nuclear and mitochondrial gene expression in organelle biogenesis. *Proc Natl Acad Sci USA* 91: 1309 – 1313
48. Shevchenko A, Tomas H, Havlis J, Olsen JV, Mann M (2007) In-gel digestion for mass spectrometric characterization of proteins and proteomes. *Nat Protoc* 1: 2856 – 2860
49. Rappsilber J, Mann M, Ishihama Y (2007) Protocol for micro-purification, enrichment, pre-fractionation and storage of peptides for proteomics using StageTips. *Nat Protoc* 2: 1896 – 1906

50. Cox J, Mann M (2008) MaxQuant enables high peptide identification rates, individualized p.p.b.-range mass accuracies and proteome-wide protein quantification. *Nat Biotechnol* 26: 1367 – 1372
51. Tyanova S, Temu T, Cox J (2016) The MaxQuant computational platform for mass spectrometry-based shotgun proteomics. *Nat Protoc* 11: 2301 – 2319
52. Tyanova S, Temu T, Sinitcyn P, Carlson A, Hein MY, Geiger T, Mann M, Cox J (2016) The Perseus computational platform for comprehensive analysis of (prote)omics data. *Nat Methods* 13: 731 – 740
53. Dimauro I, Pearson T, Caporossi D, Jackson MJ (2012) A simple protocol for the subcellular fractionation of skeletal muscle cells and tissue. *BMC Res Notes* 5: 513
54. Edgar R, Domrachev M, Lash AE (2001) Gene Expression Omnibus: NCBI gene expression and hybridization array data repository. *Nucleic Acids Res* 30: 207 – 210
55. Vizcaino JA, Csordas A, Del-Toro N, Dianes JA, Griss J, Lavidas I, Mayer G, Perez-Riverol Y, Reisinger F, Ternent T *et al* (2016) 2016 update of the PRIDE database and its related tools. *Nucleic Acids Res* 44: 11033

